Capillarity

Vol. 13, No. 1, p. 1-9, 2024

Original article

Impeding effect on droplet spreading by a groove on the substrate

Xin Huang[1], YingQi Li[2]*, JingCun Fan[1], HengAn Wu[1], FengChao Wang[1]*

[1]*Department of Modern Mechanics, University of Science and Technology of China, Hefei 230027, P. R. China*
[2]*Department of Mechanics, Sichuan University, Chengdu 610000, P. R. China*

Keywords:
Capillary force
contact line
groove
pinning force
molecular dynamics simulations

Cited as:
Huang, X., Li, Y. Q., Fan, J. C., Wu, H. A., Wang, F. C. Impeding effect on droplet spreading by a groove on the substrate. Capillarity, 2024, 13(1): 1-9.
https://doi.org/10.46690/capi.2024.10.01

Abstract:
Understanding the wetting behaviors of droplets on grooved surfaces is indispensable in surface science and offers promising avenues for advancing industrial processes. The droplet spreading on grooved surfaces can be discretized into a series of individual events that the droplet across each groove with variations in capillary forces and a subsequent re-equilibrium. In this work, a simplified model of droplet spreading on surface with an individual groove on both the left and right sides was utilized in order to elucidate the fundamental mechanisms underlying contact line pinning due to the groove. We examined the effects of the groove position and the wettability of solid surfaces. The contact line is observed to be pinned when the grooves are strategically positioned. However, by reducing the distance between the grooves, the contact lines can cross them. In such instances, the spreading process can be classified into four modes: Free spreading, impeding spreading, pinning, and depinning. The pinning and depinning phenomenon are explained by the balance between the driving force and pinning force on the contact line. Based on simulation results, the maximum pinning force exerted on the contact line by a certain solid surface can be theoretically predicted. Besides, the wettability of the solid surface also contributes to the impeding effect. This work provides theoretical guidance for the study of wetting on grooved surfaces at the nanoscale, which is essential for developing a comprehensive understanding of the interactions between droplets and structured surfaces, with potential applications in optimizing industrial processes and advancing surface science.

1. Introduction

Wetting, a fundamental concept in surface science and fluid dynamics, refers to the interaction between a liquid and a solid surface. This phenomenon is governed by the balance of adhesive and cohesive forces, influencing how a liquid spread or adhere to a given substrate (De Gennes et al., 2004; Bonn et al., 2009). The study of wetting has garnered considerable attention due to its ubiquitous presence in both everyday life and industrial applications. On the nanoscale, where the surface area to volume ratio becomes highly significant, surface forces, molecular interactions, and quantum effects play a dominant role (Zarzar et al., 2015; Wang et al., 2022b; Zhang et al., 2023). Wetting at the nanoscale is crucial in designing advanced materials with specific properties, impacting domains such as nanofluidic, oil extraction and biomimetics (Zhao et al., 2016; Cherukupally et al., 2021; Wang et al., 2022a). Understanding the droplet spreading on the nanoscale allows for the tailoring of surfaces to achieve desired functionalities, offering unprecedented opportunities for innovation in nanotechnology.

Surface wettability is the intrinsic characteristic of a solid that dictates its capacity to either attract or repel a liquid. This property is influenced by multiple factors, including surface chemistry (Zhang et al., 2015), surface roughness (Fan et al., 2021), and surface defects (Perrin et al., 2016). The strate-

Yandy Scientific Press

*Corresponding author.
E-mail address: huangx2021@mail.ustc.edu.cn (X. Huang); liyq@scu.edu.cn (Y. Li); fanjc@ustc.edu.cn (J. Fan); wuha@ustc.edu.cn (H. Wu); wangfc@ustc.edu.cn (F. Wang).

Received May 30, 2024; revised June 19, 2024; accepted July 10, 2024; available online June 16, 2024.

gic control of surface structures on the nanoscale serves as a powerful tool to achieve specific wetting behaviors (Paxson and Varanasi, 2013; Zhao, 2014; Sarshar et al., 2019). Some researchers have attempted to study the spreading behavior of liquid droplets on grooved surfaces. Experimental investigations have revealed that the spreading dynamics of droplets on a micro-grooved surface are primarily dominated by the capillary force (Ding et al., 2022). Moreover, the wetting shape of the droplet is linked to its base area (Yang et al., 2009). The anisotropy wetting behaviors were observed on sinusoidal micro-grooved surfaces, with the equilibrium contact angle across the grooves significantly larger than that parallel to the grooves (Qi et al., 2018). The experimental exploration of droplet movement on surface with V-shaped grooves has revealed a transition of droplets from an immersed state to a suspended state with decreasing cross-sectional angles of V-shaped grooves (Xu et al., 2016). Understanding the spreading behavior of liquid droplets on structured surfaces has become a topic of significant interest due to its critical applications in fields such as microfluidics (Wang et al., 2015).

The wetting state is primarily controlled by the contact line, a tiny liquid corner where three phases intersect, spanning only a few atomic distances and bearing capillary forces (Gao and McCarthy, 2007; Fan et al., 2020). The contact line plays an important role in controlling the wetting state by determining the equilibrium shape and spreading dynamics of the droplet. The behavior of the contact line, whether it remains pinned, moves, or undergoes depinning, significantly influences the wetting dynamics. The movement and stability of the contact line are governed by a complex interplay of adhesive and cohesive forces, capillary forces, and viscous forces (Cai et al., 2021, 2022; Liu and Wang, 2022). Understanding this force balance at the contact line is crucial for unraveling wetting phenomena such as pinning and depinning (Liu et al., 2014; Teshima et al., 2017). Pinning occurs when the contact line resists movement due to a delicate balance between adhesive and capillary forces, while depinning refers to the initiation of contact line motion. Experimental studies have focused on characterizing the forces acting on the contact line. On pillared surfaces, the spacing between adjacent pillars influences the forces experienced by the contact line, wherein an increase in this spacing leads to a proportional increment in the force acting on the contact line (Paxson and Varanasi, 2013). The increased wettability of the solid substrate leads to a larger pinning force for a droplet on a chemically homogeneous surface (Putnam et al., 2012). On surfaces featuring multiple grooved structures, each instance of droplet spreading across a groove represents a change and subsequent rebalancing of forces (Yada et al., 2021). Consequently, our investigation aims to delve into the wetting of the contact line crossing an individual groove, elucidating the fundamental principles underlying contact line pinning and its mechanisms. Basic theories of pinning phenomenon at the contact line are essential to the control and applications of nanofluids on grooved surface.

In this study, the spreading and wetting behaviors of droplets are investigated when residing on surfaces with an individual groove on both the left and right sides of the surface, respectively. We examined the impact of varying distance between the left and right grooves and distinct wetting properties of the solid-liquid interface on droplet wetting. Molecular dynamics (MD) simulations were applied to study the spreading process and the equilibrium state of a droplet on surface with grooves. The contact angle and the capillary force on the contact line were analyzed to elucidate the spreading process of the droplet. The force balance on the contact line determines whether the contact line continues to spread or is pinned by the surface. This work provides theoretical guidance for wetting on the grooved surface.

2. Methodology and simulations

2.1 Model

The model of a liquid droplet spreading on solid surfaces with grooves were employed to highlight the effect of an individual groove on the contact line motion. Here, the solid substrate was constructed using a simple cubic lattice, with a lattice constant of $a_0 = 0.28$ nm. The dimensions of the solid substrate were $80a_0 \times 13a_0 \times 7a_0$. Rectangular grooves were symmetrically carved on both sides of the solid surface, with a varying distance denoted as L, which was shown in Fig. 1(a). The dimensions of each groove were $3a_0 \times 13a_0 \times 3a_0$. A liquid droplet was modeled containing 6,075 argon atoms with its initial radius 5.0 nm. Periodic boundary conditions were employed in the x and y directions leading to the droplets taking the shape of a long columnar cap. The droplet was first placed approximately 0.2 nm away from the substrate, then it came into contact with the solid and spread. The change in the center of mass of the droplet in the z direction was monitored to determine whether the droplet had reached its equilibrium state. Meanwhile, a comparative analysis of a droplet spreading on a smooth surface was conducted, which further highlighted the impeding effect on the spreading due to the presence of a groove.

2.2 Molecular dynamics simulations

During the MD simulations, the atomic interactions were modeled by the standard 12/6 Lennard-Jones pairwise potential. The potential energy was calculated by the following formula:

$$U(r_{ij}) = 4\chi_{AB}\varepsilon_{ij}\left[\left(\frac{\sigma_{ij}}{r_{ij}}\right)^{12} - \left(\frac{\sigma_{ij}}{r_{ij}}\right)^{6}\right] \quad (1)$$

where ε_{ij} characterizes the strength of interactions, σ_{ij} stands for the effective size of particles, χ_{AB} is a varying coefficient to adjust the magnitude of the interaction potential energy between different atomic types, and r_{ij} is the distance between atoms i and j. In our simulations, $\sigma = 0.34$ nm and $\varepsilon/k_B = 120$ K (Huang et al., 2023), where k_B is the Boltzmann constant. For liquid-liquid interactions, $\chi_{LL} = 1.0$, while for solid-solid interactions, $\chi_{SS} = 0.0$. The solid atoms were fixed at their original position. Values of χ_{SL} were set to 0.30, 0.35 and 0.40 for solid-liquid interactions, resulting in equilibrium contact angles of 101.4°, 87.3° and 75.0° for droplets on a smooth surface, respectively. For simplicity, these surfaces were denoted as surfaces $S_{0.30}$, $S_{0.35}$ and $S_{0.40}$, respectively.

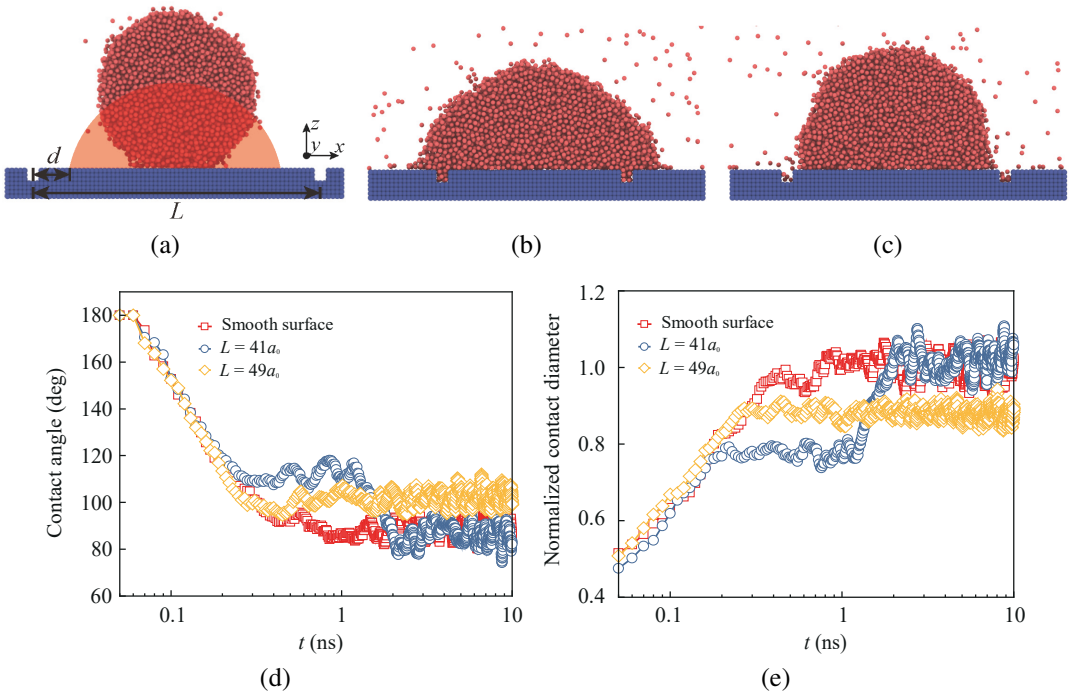

Fig. 1. (a) Molecular model of a nano-droplet on a solid surface. The transparent region indicates the equilibrium shape of a droplet residing on a smooth surface. L is the distance between the left and right grooves. d is the distance between the groove and the equilibrium position of a contact line, (b) and (c) equilibrium states of the nano-droplet on $S_{0.35}$ surface for $L = 41a_0$ and $49a_0$, respectively, (d) evolution of the contact angle versus spreading time on $S_{0.35}$ surface for $L = 41a_0$ and $49a_0$ and (e) evolution of the contact diameter versus spreading time on $S_{0.35}$ surface for $L = 41a_0$ and $49a_0$. The contact diameters are normalized by the equilibrium value of the droplet on a smooth surface.

All the interactions were considered within a cutoff of $r_c = 1.8$ nm.

The size of the simulation box was 22.4 nm × 3.64 nm × 13.0 nm and the length of the simulation box in the x-direction was long enough to prevent the interactions between the droplet and its periodic mirror images. The line tension effect could be neglected (Lukyanov, 2022). The simulations were conducted in canonical ensembles with a Nose-Hoover thermostat to control the temperature at 90 K. The time step was set to be 1.0 fs. All MD simulations were performed using Large-scale Atomic/Molecular Massively Parallel Simulator (Plimpton, 1995).

2.3 Contact angle & capillary force measurement

To calculate the contact angle θ, the time-averaged liquid density is computed in the x-z plane. The liquid-vapor interface was distinguished by a threshold of $0.5\rho_{\text{bulk}}$, where ρ_{bulk} was the density of bulk liquid. A layered structure of liquid formed near the solid substrate due to solid-liquid interactions (Ruckenstein and Berim, 2010), which should be disregarded in advance. Subsequently, the droplet profile was determined by fitting a circular arc to the liquid-vapor interface, excluding the layered structure (3 layers). Finally, the contact angle was defined by measuring the tangent of this circular arc at the solid (Ingebrigtsen and Toxvaerd, 2007).

When analyzing the forces on the contact line, there exists a capillary force balance proposed in our previous work (Fan et al., 2020). Here the capillary force is defined as the attractive force exerted on the contact line by the solid substrate (Fan et al., 2020). We first calculated the forces exerted by the liquid atoms on the solid atoms (Seveno et al., 2013). The solid substrate was meshed along the x direction with a width of a_0, where each mesh grid contained a single column of solid atoms along the x-axis. Then the tangential capillary forces $\tau_{||}$ on the solid were time-averaged on each mesh grid. For simplicity, the region of the grooves is excluded to measure the capillary force on the contact line. We integrated $\tau_{||}$ along the x direction from the center of the droplet to the positions of the contact lines on both sides. The mean value was considered as the capillary force F_S. The time-averaged interval of both the liquid density and the capillary force is 12×10^6 timesteps (12 ns).

3. Results

3.1 The wetting behavior

After the nano-droplet came into contact with the solid, it began spreading. During this process, both the contact angle and the distance between two contact lines (referred to as the contact diameter subsequently) are measured. We found that only when the grooves were positioned at an appropriate location, they act as physical barriers that hinder the spreading. In other words, the constraint effect on the contact line motion

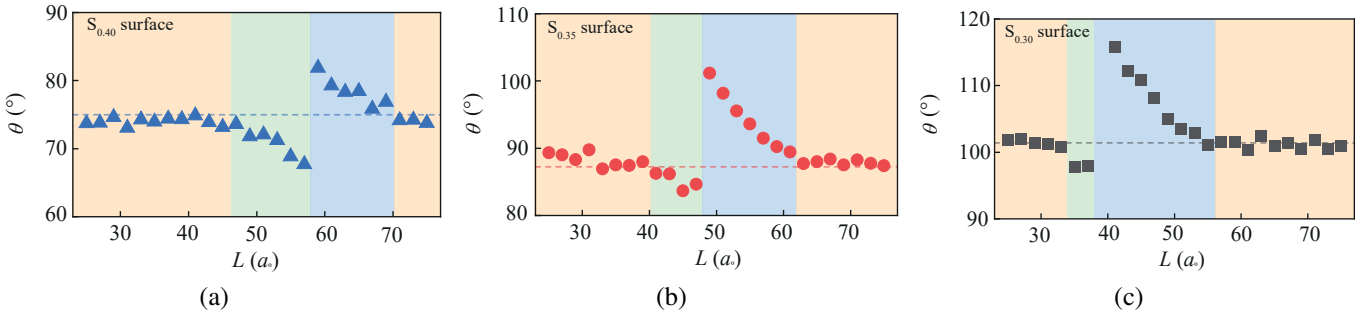

Fig. 2. The equilibrium contact angle (θ) of a droplet on the (a) $S_{0.40}$, (b) $S_{0.35}$ and (c) $S_{0.30}$ surfaces. The dashed lines represent the equilibrium contact angle of the same droplet on a smooth surface. The blue region indicates the pinning range, the green region indicates the depinning range, and the orange region indicates where the contact lines are unaffected by the grooves.

by the groove depends on L. In the initial stages of spreading, there exists a driving force resulting from the unbalanced capillary forces, $\gamma_{LV}(\cos\theta_t - \cos\theta_0)$ where γ_{LV} is the liquid-vapor interface tension, θ_t is the instant contact angle and θ_0 is the equilibrium contact angle on a smooth surface. This driving force is much greater than the maximum pinning force that a solid substrate and the groove can provide. The instantaneous contact angle will continue to decrease, leading to the decreasing driving force on the contact line. If the contact line meets the groove before the decreasing driving force becomes smaller than the pinning force provided by the groove, it can still cross the groove, albeit with certain constraints. On the contrary, the contact line would be pinned at the groove because the driving force is not large enough. The evolutions of the contact angles and the contact diameters of two typical constrained spreading behaviors are presented in Fig. 1(d) and Fig. 1(e) for the cases on the surface $S_{0.35}$ with $L = 41a_0$ and $49a_0$, respectively, which were compared with the spreading behaviors of the same droplet but on a smooth solid surface.

When $L = 41a_0$, the spreading behavior encountered constraints imposed by surface grooves. However, as the droplet spread, the liquid would gradually overcome these constraints, ultimately crossing the grooves. Initially, the contact angle decreased rapidly while the contact diameter increased quickly as the droplet spread on the surface. This process exhibits no significant difference compared to the spreading on the smooth surfaces, which is referred to as the free spreading. Subsequently, as the contact lines approached the grooves, the spreading behavior became more intricate. Ultimately, the droplet reached an equilibrium state where the contact angle and contact diameter stabilize.

In another typical spreading scenario, $L = 49a_0$, the contact lines are unable to cross the grooves. After the free spreading, the contact lines were pinned at edge of the grooves. The droplet attained an equilibrium state characterized by the stabilized contact angle and contact diameter. The duration for droplet spreading to reach equilibrium was shorter compared to the first scenario. Due to differences in the strength of the solid-liquid interface, the locations where the contact line is pinned were different, and the intensity of the pinning effect varies. Nevertheless, despite these differences, the spreading process of a droplet on surfaces $S_{0.30}$ and $S_{0.40}$ demonstrated a similar behavior.

To further analyze the spreading behaviors on surfaces with grooves, the equilibrium contact angle of droplets are calculated with varying solid-liquid interaction coefficients and different groove spacings L, as shown in Fig. 2. In the case of a droplet on the $S_{0.40}$ surface, the variation in the equilibrium contact angle signified the pinning-depinning transition of the contact lines. Initially, θ remains constant when $L > 71a_0$, indicating that the contact lines remain unaffected because the contact line does not meet the grooves. As L is decreasing, the contact lines are pinned by the grooves, leading to an increasing contact angle. If the contact line meets the groove with a large enough driving force on it (large current contact angle), the contact lines will cross the groove, yet the equilibrium angle is slightly lower than that on a smooth surface. For the case that the grooves are inside the droplet and are far away from the contact lines ($L < 45a_0$), the contact angle stabilized at a value equivalent to that on a smooth surface, signifying that the contact lines were not influenced by the grooves. Consistent tendencies were observed in the cases of a droplet placed on the $S_{0.35}$ and $S_{0.30}$ surfaces.

Additionally, it can be found that L possesses a certain range (referred to as the pinning range) within which the contact line remains pinned. The pinning range characterizes the strength of the pinning effect on the contact line. As L continuously decreases, the pinning effect intensifies until the contact lines are able to cross the grooves. This specific range of pinning indicates that the pinning effect has an upper limit. Meanwhile, there exists a range of L where the contact line is depinning (referred to as the depinning range). Here, the contact line depinning denotes the phenomenon where the contact angle is influenced by the presence of grooves even after the contact lines has crossed them. The depinning ceases when the contact angle is restored to its equilibrium value, as observed for a droplet on a smooth surface.

By comparing the equilibrium states of droplets on surfaces with different wettability, it can be found that the pinning and depinning range varied with the wettability of the solid-liquid interface. The pinning range exhibits an expansion with

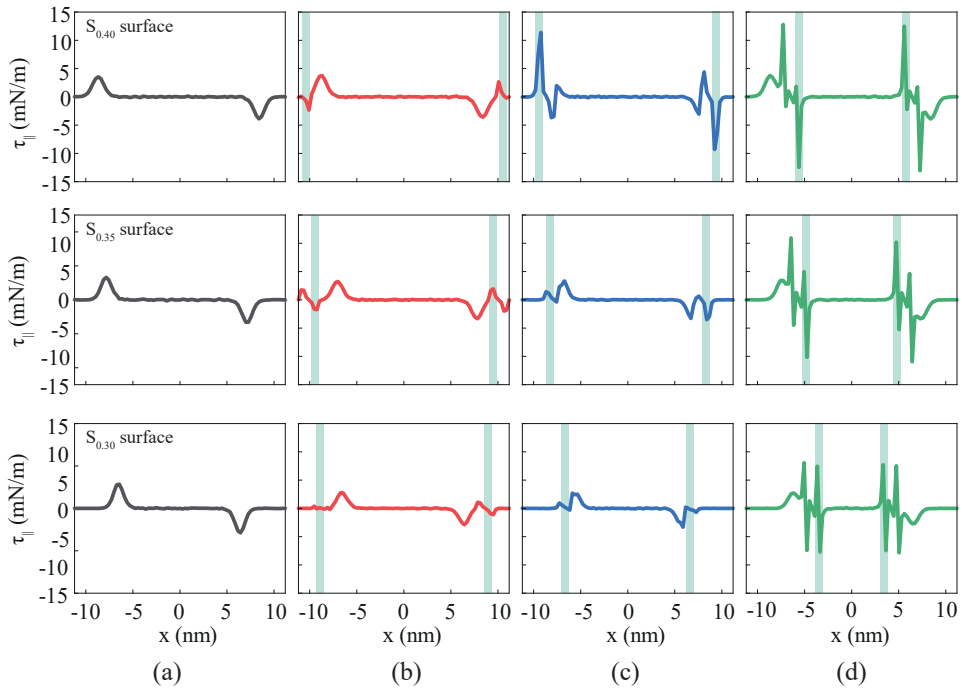

Fig. 3. The distribution of the tangential capillary force ($\tau_{||}$) of a droplet on different surfaces. From top to bottom, the three rows of images correspond to the $S_{0.40}$, $S_{0.35}$ and $S_{0.30}$ surfaces, respectively. The shaded regions indicate the positions of the grooves. The results on some representative surfaces were presented: (a) On a smooth surface, (b) when far from the contact line, $d = -8a_0$, (c) when pinned by the grooves, $d = 0$ and (d) when inside the droplet, $d = 8a_0$.

a decrease in the wettability of the solid-liquid interface, while the depinning range demonstrates a reduction. The pinning and depinning phenomenon can be understood through the principle of minimizing interfacial energy. Grooves on the surface result in the local minima and maxima in the interfacial energy of the entire system. When the contact line encounters a groove, it experiences an energy barrier. If the energy barrier is greater than the free energy of the contact line, the contact line is pinned there. While if the energy barrier can be overcome, the contact line will move past the groove. In such cases, the droplet seeks to minimize its overall interfacial energy. This process continues until the contact line reaches another energy barrier or the system achieves an equilibrium state where the interfacial energy is minimized. The wettability of the solid surface, which is determined by the solid-liquid interaction, affects the height of the energy barriers. Surfaces with lower wettability exhibit higher solid-liquid interfacial energy as the liquid tends to minimize its contact with the solid. This results in a larger energy barrier that must be overcome for the droplet to move or spread. Consequently, the contact line becomes more easily pinned as it encounters substantial energy barriers when attempting to traverse surface groove. Furthermore, on surfaces with lower wettability, even after the contact line progresses past a groove, the elevated interfacial energy continues to influence the contact angle.

3.2 The tangential capillary force

We also computed the tangential capillary force $\tau_{||}$ exerted by the liquid on the solid atoms, as depicted in Fig. 3. Compared with the droplet on a smooth surface (Fig. 3(a)), the droplet on surface with grooves (Figs. 3(b)-3(d)) exhibited a different distribution of the tangential capillary force. We investigated the influence of the distance between the groove and the equilibrium position of a contact line, denoted as d. Here, d is positive when the groove is inside the droplet and negative when the groove is outside the droplet. For the cases that the grooves were positioned outside the droplet, located at a considerable distance from the contact lines (Fig. 3(b)), interactions between solid and liquid atoms led to the adsorption of liquid atoms within the grooves. Consequently, $\tau_{||}$ was not zero near the grooves. The stronger the solid-liquid interaction coefficients, the more liquid atoms were adsorbed into the grooves. But this force peak originating from the grooves did not affect the contact lines, namely, did not contribute to the capillary force acting on the contact line. When the contact lines were pinned by the grooves (Fig.3(c)), the distribution of $\tau_{||}$ changed. There existed two force peaks on each side, exhibiting consistent directions on both sides. The outer peak was attributed to the presence of grooves, whereas the inner peak arose from the influence of the contact line. When the grooves were inside the contact lines (Fig. 3(d)), fluctuations were observed at the groove locations. The liquid atoms distributed left-right symmetrically around each groove, ensuring that the resultant force on the solid equal to zero. The actual capillary force originating from the contact line was manifested by the outer force peak.

The integrated tangential capillary force F_S was shown in Fig. 4. For the cases the grooves were positioned outside of the

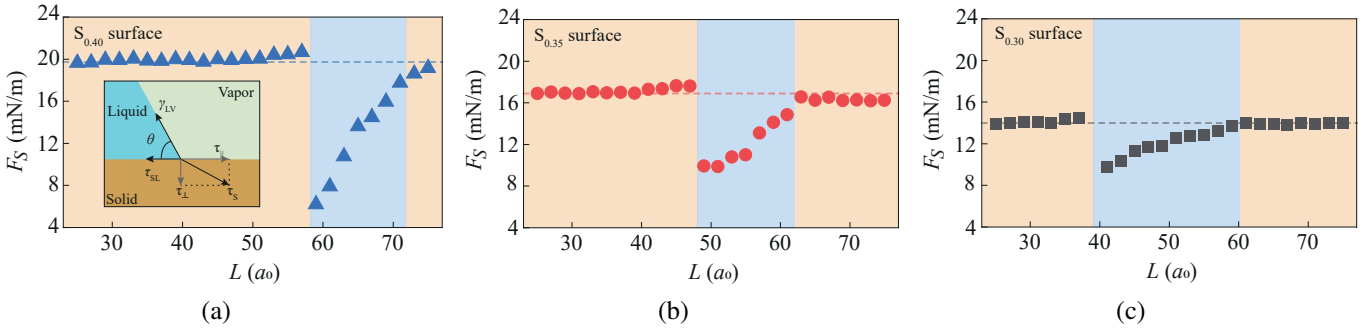

Fig. 4. The integrated tangential capillary force (F_S) of the droplet on the (a) $S_{0.40}$, (b) $S_{0.35}$ and (c) $S_{0.30}$ surfaces. The dashed lines represent the equilibrium value of the same droplet on a smooth surface. The inset is the sketch of the capillary force balance at the contact line.

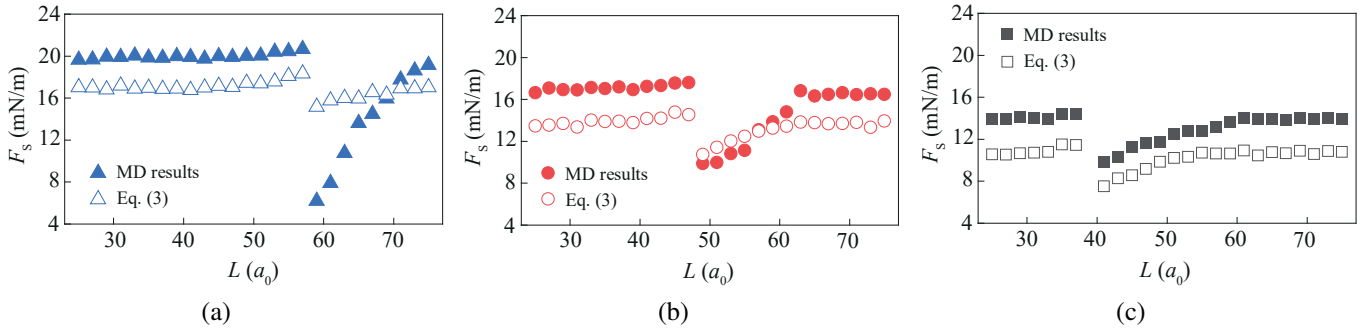

Fig. 5. The comparison between the tangential capillary force (F_S) obtained from Eq. (3) and MD simulations of a droplet on the (a) $S_{0.40}$, (b) $S_{0.35}$ and (c) $S_{0.30}$ surfaces.

droplet, the integration of $\tau_{||}$ are conducted from the center of the droplet to the positions of the contact lines on both sides. The region of the grooves was excluded and the resulting value F_S represented the capillary force from the contact line. For the case that the grooves were at the inside of the droplet, $\tau_{||}$ are directly integrated from each side. In the circumstance of a droplet on the $S_{0.40}$ surface, F_S remained constant when the grooves were positioned far from the contact lines, regardless of whether they were positioned inside or outside the droplet. In this scenario, the equilibrium state of the droplet remained unaffected by the grooves, with the capillary force experienced by the contact lines remaining consistent with that observed on a smooth surface. With an increase in L, the equilibrium state of the droplet became constrained by the grooves, preventing the contact lines from crossing them. In the initial state of pinning, the pinning effect was strongest, resulting in the maximum contact angle and the least capillary force exerted on the contact line. As L increases, the droplet gradually relaxed, and F_S gradually increased. Consistent tendencies were found in the droplet on the $S_{0.35}$ and $S_{0.30}$ surfaces.

The variations in tangential capillary force differ from those in the contact angles, primarily concentrating on the contact line pinning. Once the contact lines are able to cross across the groove, the distribution of liquid atoms on both sides of the grooves exhibits local left-right symmetry, ensuring that the resultant force on the grooves equal to zero. Consequently, in such cases, the capillary force acting on the contact line is identical to that on a smooth surface. However, changes in contact angles reflect both pinning and depinning phenomena. Even after the contact line crosses the groove, it remains subject to nearby geometric constraints, leading to deviations from the equilibrium contact angle. This constraint effect weakens as the contact line gradually moves away from the groove, resulting in the depinning phenomenon.

4. Discussions

Young's equation is a fundamental tool for describing and predicting the wetting behavior at the contact line:

$$\gamma_{SV} - \gamma_{SL} = \gamma_{LV} \cos\theta \tag{2}$$

where γ_{SV} and γ_{LV} are the solid-vapor and liquid-vapor interface tensions, respectively and θ is the equilibrium contact angle. For the equilibrium state of a droplet, there is a capillary force balance at the contact line (Seveno et al., 2013; Fan et al., 2020). In the tangential direction, it can be described as following:

$$F_S = \gamma_{LV} (1 + \cos\theta) \tag{3}$$

This explains why, when the contact line is pinned, a larger contact angle result in a smaller capillary force. A comparative analysis between the tangential capillary force F_S obtained from Eq. (3) and the MD results is presented in Fig. 5. In instances where the solid surface is lyophobic, Eq. (3) reliably

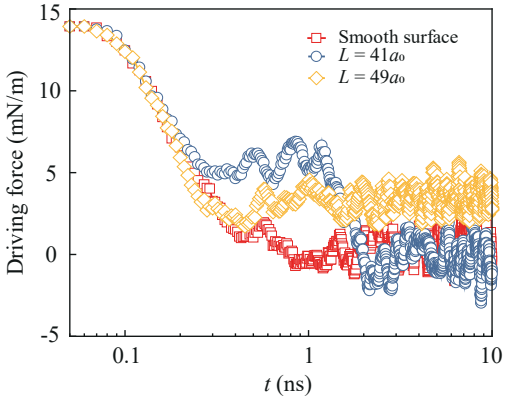

Fig. 6. Evolution of the driving force versus spreading time on $S_{0.35}$ surface for $L = 41a_0$ and $49a_0$.

predicts the tangential capillary force. However, when the solid surface is lyophilic, Eq. (3) yields slightly different results in predicting the pinning of the contact line. This discrepancy arises from stronger solid-liquid interactions, leading to a greater number of liquid atoms being adsorbed within surface grooves, forming a quasi-prewetting layer. Under thermal agitation, liquid within the grooves is able to surpasses the energy barrier imposed by the grooves, resulting in an exchange of liquid with that along the contact line. Consequently, the calculated values of the capillary force tend to underestimate the actual force.

The equilibrium state of droplet is determined by the force balance on the contact line. Owing to the out-of-balance surface tension force, there exists a driving force on the contact line during droplet spreading (Blake, 2006):

$$F_{\text{driving}} = \gamma_{LV}(\cos\theta_t - \cos\theta_0) \tag{4}$$

where θ_t is the current contact angle and θ_0 is the equilibrium contact angle on a smooth surface. This driving force minimizes the energy of the droplet by adjusting the contact angle, thereby promoting the spreading of the droplet. Meanwhile, the solid surface applies a pinning force on the contact line, impeding its further expansion and constraining the droplet's morphology. This pinning force is a reaction force of the driving force, with a maximum limit determined by the solid surface (White and Schmucker, 2021). The grooves on the surface can enlarge this maximum pinning force, highlighting the pinning phenomenon of the contact lines. These two forces compete with each other, jointly determining the state of the contact line.

The competition relationship between the driving force and the pinning force has a significant effect on the motion of the contact line during the spreading process. The evolutions of the driving force during spreading on $S_{0.35}$ surface for two typical scenario are shown in Fig. 6. At the beginning of the spreading, the driving force, determined by a high value of the contact angle, significantly exceeded the pinning force. Consequently, the droplet spread continuously on the surface. As the contact lines approached the grooves, the pinning force provided by the solid surface increased. In both scenarios, $L = 41a_0$ and $49a_0$, the maximum pinning forces remained the same, as the grooves on the substrate have identical dimensions, differing only in their positions. In the case of $L = 41a_0$, the contact lines encountered the grooves earlier than that in the latter case, implying that the contact lines experienced a greater driving force. As the driving force acting on the contact line still exceeded the maximum pinning force, the contact line crossed the groove.

Conversely, in the case of $L = 49a_0$, where the driving force failed to surpass the maximum pinning force, the contact lines became pinned by the grooves. In such instance, although the driving force retained a relatively high value owing to surface tension, it was balanced by the pinning force, resulting in the phenomenon of contact line pinning. In other word, the pinning force on the contact line should be the same as the driving force, when the contact line is fixed.

For a droplet spreading on a surface, its initial volume is predetermined. Thus, by strategically designing the distance L between two grooves, the contact angle of the droplet can be controlled when it encounters the grooves, thereby determining the equilibrium state of the droplet. Specifically, when the droplet encounters the grooves with a sufficiently large contact angle, the contact line overcomes the energy barrier imposed by the grooves under the effect of driving force, and the contact line succeed to cross them. However, if the contact angle is insufficient to generate enough driving force to overcome the energy barrier, the droplet becomes pinned by the grooves. Therefore, whether the droplet is pinned or not depends on its volume and the designed distance L.

Fig. 2 shows the range of L values and the corresponding contact angles for which the droplet can be pinned by the grooves. Applying Eq. (4), we can obtain the driving forces acting on the contact line, which reflects the values of the pinning force. Previous research revealed that the pinning force provided by the solid surface is a self-mediated force to maintain the balance on the contact line (Huang et al., 2023). This explain why the pinning force is not a constant but varies depending on the pinning state.

What matters is the maximum pinning force that the solid surface can provide. Here, the grooves on the solid surface are applied to strengthen this maximum pinning force. The value of the maximum pinning force depends on the wettability of the solid surface. The stronger the solid-liquid interaction, the more easily the liquid spreads and flows on the solid surface, reducing the effectiveness of surface microstructures in pinning the liquid. Consequently, the maximum pinning force that the solid can provide decreases. On the other hand, stronger wettability reduces the contact angle hysteresis, resulting in a smaller pinning force. We can predict the maximum pinning force by analyzing the moment right before the contact line cross the groove. Since the droplet is pinned, which means that the pinning force should be equal to the driving force on the contact line. We can thus measure the contact angle at this moment and using Eq. (4) to obtain the maximum pinning force. This provides us an approach to compute the pinning force using the force balance on the contact line when the contact line is pinned.

5. Conclusion

In this work, the spreading dynamics and the equilibrium states of a droplet are investigated on surfaces featuring individual grooves positioned on both the left and right sides. We examined the influence of varying distances between the left and right grooves and the distinct wetting properties of the solid-liquid interface. Our observations reveal that strategically positioned grooves can lead to the pinning of the contact line. However, reducing the distance between the grooves enables the contact lines to cross them. In such instances, the spreading process can be categorized into four modes: Free spreading, impeding spreading, pinning, and depinning. Additionally, it can be found that the wettability of the solid surface also contributes to the pinning effect. Specifically, the stronger the wettability of the solid surface, the weaker the ability of the contact line pinning.

This study also revealed the distributions of the tangential capillary force experienced by the contact line on the surface with grooves. The Young's equation on the contact line has been verified at such case. The pinning and depinning phenomenon are explained by the balance between the driving force and pinning force on the contact line. The driving force and the pinning force jointly determine the state of the contact line. The primary cause of continuous spreading is when the driving force surpasses the maximum pinning force provided by the surface. If not, then the contact line will be pinned on the solid surface. Based on simulation results, it provides a method to theoretically predict the maximum pinning force exerted on the contact line by a certain solid surface. This work provides theoretical insights for wetting on the grooved surface.

Acknowledgements

This work was financially supported by National Key R&D Program of China (No. 2019YFA0708700), National Natural Science Foundation of China (Nos. 12241203 and U22B2075), and the Youth Innovation Promotion Association CAS (No. 2020449). The numerical calculations were performed on the supercomputing system in Hefei Advanced Computing Center and the Supercomputing Center of University of Science and Technology of China.

Conflict of interest

The authors declare no competing interest.

References

Blake, T. D. The physics of moving wetting lines. Journal of Colloid and Interface Science, 2006, 299(1): 1-13.

Bonn, D., Eggers, J., Indekeu, J., et al. Wetting and spreading. Reviews of Modern Physics, 2009, 81(2): 739-805.

Cai, J., Chen, Y., Liu, Y., et al. Capillary imbibition and flow of wetting liquid in irregular capillaries: A 100-year review. Advances in Colloid and Interface Science, 2022, 304: 102654.

Cai, J., Jin, T., Kou, J., et al. Lucas-Washburn equation-based modeling of capillary-driven flow in porous systems. Langmuir, 2021, 37(5): 1623-1636.

Cherukupally, P., Sun, W., Williams, D. R., et al. Wax-wetting sponges for oil droplets recovery from frigid waters. Science Advances, 2021, 7(11): eabc7926.

De Gennes, P. G., Brochard-Wyart, F., Quéré, D. Capillarity and Wetting Phenomena: Drops, Bubbles, Pearls, Waves. New York, USA, Springer, 2004.

Ding, Y., Jia, L., Yin, L., et al. Anisotropic wetting characteristics of droplet on micro-grooved surface. Colloids and Surfaces A: Physicochemical and Engineering Aspects, 2022, 633: 127850.

Fan, J., De Coninck, J., Wu, H., et al. Microscopic origin of capillary force balance at contact line. Physical Review Letters, 2020, 124(12): 125502.

Fan, J., De Coninck, J., Wu, H., et al. A generalized examination of capillary force balance at contact line: On rough surfaces or in two-liquid systems. Journal of Colloid and Interface Science, 2021, 585: 320-327.

Gao, L., McCarthy, T. J. How Wenzel and Cassie were wrong. Langmuir, 2007, 23(7): 3762-3765.

Huang, X., Fan, J., Wu, H., et al. Local molecular asymmetry mediated self-adaptive pinning force on the contact line. Colloids and Surfaces A: Physicochemical and Engineering Aspects, 2023, 674: 131987.

Ingebrigtsen, T., Toxvaerd, S. Contact angles of Lennard-Jones liquids and droplets on planar surfaces. The Journal of Physical Chemistry C, 2007, 111(24): 8518-8523.

Liu, F., Wang, M. Trapping patterns during capillary displacements in disordered media. Journal of Fluid Mechanics, 2022, 933: A52.

Liu, Y., Wang, J., Zhang, X., et al. Contact line pinning and the relationship between nanobubbles and substrates. The Journal of Chemical Physics, 2014, 140(5): 054705.

Lukyanov, A. V. Non-locality of the contact line in dynamic wetting phenomena. Journal of Colloid and Interface Science, 2022, 608: 2131-2141.

Paxson, A. T., Varanasi, K. K. Self-similarity of contact line depinning from textured surfaces. Nature Communications, 2013, 4(1): 1492.

Perrin, H., Lhermerout, R., Davitt, K., et al. Defects at the nanoscale impact contact line motion at all scales. Physical Review Letters, 2016, 116(18): 184502.

Plimpton, S. Fast parallel algorithms for short-range molecular dynamics. Journal of Computational Physics, 1995, 117(1): 1-19.

Putnam, S. A., Briones, A. M., Byrd, L. W., et al. Microdroplet evaporation on superheated surfaces. International Journal of Heat and Mass Transfer, 2012, 55(21-22): 5793-5807.

Qi, B., Zhou, J., Wei, J., et al. Study on the wettability and condensation heat transfer of sine-shaped micro-grooved surfaces. Experimental Thermal and Fluid Science, 2018, 90: 28-36.

Ruckenstein, E., Berim, G. O. Microscopic description of a drop on a solid surface. Advances in Colloid and

Interface Science, 2010, 157(1-2): 1-33.

Sarshar, M. A., Jiang, Y., Xu, W., et al. Depinning force of a receding droplet on pillared superhydrophobic surfaces: Analytical models. Journal of Colloid and Interface Science, 2019, 543: 122-129.

Seveno, D., Blake, T. D., De Coninck, J. Young's equation at the nanoscale. Physical Review Letters, 2013, 111(9): 096101.

Teshima, H., Nishiyama, T., Takahashi, K. Nanoscale pinning effect evaluated from deformed nanobubbles. The Journal of Chemical Physics, 2017, 146(1): 014708.

Wang, F., Qian, J., Fan, J., et al. Molecular transport under extreme confinement. Science China Physcis, Mechanics & Astronomy, 2022a, 65(6): 264601.

Wang, Y., Li, Z., Elhebeary, M., et al. Water as a "glue": Elasticity-enhanced wet attachment of biomimetic microcup structures. Science Advances, 2022b, 8(12): eabm9341.

Wang, S., Wang, T., Ge, P., et al. Controlling flow behavior of water in microfluidics with a chemically patterned anisotropic wetting surface. Langmuir, 2015, 31(13): 4032-4039.

White, E. B., Schmucker, J. A. Wind-and gravity-forced drop depinning. Physical Review Fluids, 2021, 6(2): 023601.

Xu, W., Lan, Z., Peng, B., et al. Directional movement of droplets in grooves: Suspended or immersed?. Scientific Reports, 2016, 6(1): 18836.

Yada, S., Allais, B., Wijngaart, W., et al. Droplet impact on surfaces with asymmetric microscopic features. Langmuir, 2021, 37(36): 10849-10858.

Yang, J., Rose, F. R., Gadegaard, N., et al. Effect of sessile drop volume on the wetting anisotropy observed on grooved surfaces. Langmuir, 2009, 25(5): 2567-2571.

Zarzar, L. D., Sresht, V., Sletten, E. M., et al. Dynamically reconfigurable complex emulsions via tunable interfacial tensions. Nature, 2015, 518(7540): 520-524.

Zhang, J., Ding, W., Hampel, U. How droplets pin on solid surface. Journal of Colloid and Interface Science, 2023, 640: 940-948.

Zhang, J., Müller-Plathe, F., Leroy, F. Pinning of the contact line during evaporation on heterogeneous surfaces: Slowdown or temporary immobilization? Insights from a nanoscale study. Langmuir, 2015, 31(27): 7544-7552.

Zhao, B., MacMinn, C. W., Juanes, R. Wettability control on multiphase flow in patterned microfluidics. Proceedings of the National Academy of Sciences, 2016, 113(37): 10251-10256.

Zhao, Y. Moving contact line problem: Advances and perspectives. Theoretical and Applied Mechanics Letters, 2014, 4(3): 034002.